Desalination and Water Treatment
www.deswater.com
doi: 10.5004/dwt.2022.28642

268 (2022) 89–98
August

Removal of Acid orange 7 dye in continuous fixed-bed reactor by alkaline treated eggshell: experimental and numerical modeling

S. Akazdam[a], S. Kaba[b,*], M. Chafi[a], L.H. Omari[c], H. Hiyane[b]

[a]*Laboratory of Engineering, Processes and Environment (LEPE) University Hassan II, Graduate School of Technology, El Jadida Road KM 7, B.P. 8012 Oasis, Casablanca, 20660, Morocco, emails: said.akazdam@gmail.com (S. Akazdam), mohammed.chafi@univh2c.ma (M. Chafi)*
[b]*Centre Marocain des Techniques du Cuir (CMTC), Complexes des Centres Techniques, Route BO 50, Sidi Maârouf, Casablanca, Morocco, emails: skaba@cmtc.ma (S. Kaba), hhiyane@cmtc.ma (H. Hiyane)*
[c]*LPMMAT, Faculty of Sciences Ain Chock, Hassan II University of Casablanca, B.P 5366 Maarif, Morocco, email: Lhajelhachemi.omari@univh2c.ma (L.H. Omari)*

Received 3 October 2020; Accepted 1 June 2022

ABSTRACT

In this study, experimental and numerical simulations were conducted to examine Acid orange 7 (AO7) adsorption by sodium hydroxide treated eggshells (SHTES). The tests were carried out in a continuous fixed-bed column of 10 cm. The Effects of initial dye concentration (30, 50 and 80 mg/L) and flow rate (2, 4 and 6 ml/min) on the column performance were also investigated. A two-dimensional (2D) axisymmetric mathematical model based on conservation equations of movement and species was used to predict the breakthrough curves of the fixed-bed for AO7 adsorption. The obtained experimental results were used to validate this model; a good compatibility has been noted between the numerical and experimental results of the breakthrough curves.

Keywords: Adsorption; Numerical modeling; Azo dye; Water treatment; Environment

1. Introduction

The Complexity of dye effluents treatment is one of the critical issues encountered during the manufacturing process. The leather and textile industries contain a significant variety of synthetic organic dyes, especially azo dyes [1]. Azo dyes are established in nature since their fixation rates on leather and textiles remain below 70%. They are known to be mutagenic [2], carcinogenic and toxic at low concentrations by resulting significant damages to both flora and fauna especially without an appropriate wastewater treatment processes. Therefore, the worldwide use is estimated of more than one million tons of dyes annually [3], the removal of synthetic dyes has a great concern from an environmental viewpoint. Acid orange 7 is considered as a synthetic azo dye, which is resistant to biologic degradation under aerobic conditions [4] and lacks sensitivity to light irradiation and chemical oxidation. These properties are mainly responsible for the fact that existing methods are inefficient for the removal of such dyes from wastewaters. Hence, it is important to have an appropriate and productive method to prevent the dyes from being discharged to the environment. Various techniques have been tested so far, for example, photo-degradation [5], anaerobic treatment [6], membranes with immobilized enzymes [7], coagulation [8], electrochemical oxidation [9], and adsorption [10].

Adsorption is a simple and low-cost technique which is very efficient to reduce toxic and harmful pollutants from

* Corresponding author.

liquid effluents. Among all the available adsorbents, activated carbon and silica are widely used for this purpose. These materials have high surface area and high porosity level; furthermore, they can be regenerated after several uses. On the other hand, the regeneration and activation processes increase the costs and the environmental impact of the activated carbon production that have not been fully assessed yet [11]. With the focus on the environment, new abundant, inexpensive, eco-friendly and biodegradable materials, such as wastes from food, agriculture and households gained attention of many researchers. Adsorption of dyes on spent tea leaves [3], fruit and vegetable peels [12], seed hulls [13], eggshells [14], and other materials have been studied so far. Eggshell is porous material that is useful for many environmental separation processes, including adsorption, due to its great surface area and large pore volumes. However, many studies have been reported in the literature about the effect of sodium hydroxide treatment on the properties of eggshells used in removal of azo dyes, which is the main focus of this research.

Fixed-bed adsorption has been evolved into a commonly used industrial application in wastewater treatment processes. A large number of papers describe a batch set-up of adsorption process [15], but continuous adsorption in fixed-bed column is usually the preferred set-up in industrial conditions. It is simple to manage and can be scaled-up from laboratory or pilot-plant processes [16].

The packed bed columns efficiency can be explained through breakthrough curve notion, which is the concentration profile of the adsorbate at the column outlet as a function of time. The time of breakthrough point and the shape of the breakthrough curve are crucial features of the adsorbate-adsorbent system. The first part of the breakthrough curve can be significantly affected by the axial dispersion, whilst the flux velocity can alter the shape of the second part of the curve [17]. Pseudo-kinetic models for description of fluid-solid adsorption and fluid-solid reactions are simple to use, however, Russo et al. [18] admit that the diffusive models describe better the realistic mechanisms of adsorption since they allow considering involved physical phenomena.

In adsorption, the intrinsic kinetics is faster and the adsorbate-adsorbent interaction can be considered instantaneous. So, the idea of rapid local equilibrium can be used to model the process. Hatzikioseyian et al. [18] examined such approach for mathematical modeling of adsorption in a fixed-bed column. Although mass transfer limitations exist in most sorption processes, the developed model by Hatzikioseyian et al. [19], which mainly uses an apparent dispersion coefficient of the column which was able to predict the breakthrough data.

The breakthrough curves and correlations between the experimental data and the model were used to describe the adsorption capacity of selenium on an adsorbent prepared from inactive aquatic weeds [20]. This study confirmed the linear dependence of the adsorption capacity on the inlet concentrations and good correlation between the numerical values obtained from theoretical 3D model and the experimental data.

Different approaches can be used to characterize and optimize the flow patterns inside a packed bed reactor. In fixed-bed reactors with a small ratio of tube diameter to particle diameter, models such as heterogeneous or pseudo-heterogeneous models, have some limitations because they do not consider local flow effects and heat and mass transfers [21].

Numerical simulations by finite element method were used to calculate dispersion coefficients in artificial porous media and the solution of 2D advection–dispersion equation provided good agreement with the experiment [22]. Qian et al. [23] have used 2D model based on the convection-diffusion equation and the Nernst–Planck law to simulate the breakthrough curves of adenosine-3′, 5′-cyclic monophosphate (cAMP) adsorption onto an ion-exchange resin from an aqueous solution. The comparison of the obtained numerical values from the mathematical model with the results from column experiments indicated that the model described well the breakthrough curves.

Vaiano et al. [24] investigated the fluid dynamic in a structured bed photoreactor using an N-doped TiO_2 immobilized on glass as catalyst with the aim to eliminate pollutants from wastewaters. The simulations were performed with 2D finite element model with axial symmetry. The experimental results of methylene blue degradation were compared thoroughly with the theoretical numerical values obtained from the solution of the mathematical model and the model was successfully validated. Xu and Yu [25] managed to simulate numerically gas-solid flow in a fluidized bed. The study involved understanding the fluid flow behavior in packed bed systems by solving related governing equations. A computational fluid dynamic study using the discrete particle method was used to obtain the results, which were validated with literature data and the solution of the steady-state was investigated. Zheng et al. [26] used a 2D axisymmetric geometry model to examine transport phenomena during the pressure swing adsorption (PSA) process inside an adsorber. The model reflected the compressibility of gas, heat effects, radial porosity and dead volume and the proposed geometry was a rectangular grid with approximately 11,730 quadrilateral cells. The model was compared with experimentally measured adsorption isotherms for pure oxygen and nitrogen on LiX zeolite adsorbent. The results confirmed that the model can be used to optimize the adsorber arrangement.

The numerical models have become widely used in adsorption dye treatment especially in fixed-bed reactors. Marin et al. [27] tested three mathematical models to describe the removal of reactive blue 5G dye removal by adsorption with polymeric adsorbent Dowex Optipore SD-2 in fixed-bed columns. The model that involved internal resistance and a variable mass transfer coefficient was more accurate than the other models, which took into account the external mass resistance or the adsorption in the adsorbent sites. Another model based on finite volume method discretization was successfully applied for calculations of photocatalytic decolorization of textile dyes with immobilized titania nanoparticles [28].

The primary aim of this paper is to investigate the experimental and numerical adsorption results of Acid orange 7 (AO7) on the sodium hydroxide treated eggshells (SHTES). After the preparation and the characterization of the treated adsorbent (SHTES), different experiments were carried out on the continuous fixed-bed reactor in order to optimize the working parameters, initial concentration and

flow rate. These results were compared with those of the numerical model used in the frame of this work.

2. Materials and methods

2.1. Preparation of dye solution and determination of the adsorption capacity

In this study, the used Acid orange 7 (4-(2-hydroxy-1-naphthylazo) benzene sulfonic acid sodium salt) was obtained from Merck (China). A stock solution (AO7) of 500 mg/L was prepared by dissolving the appropriate amount of dye in distilled water and further diluted to three different concentrations (30, 50 and 80 mg/L) to measure the adsorption capacity. The absorbance of AO7 solutions was measured at 485 nm using UV-visible spectrophotometer Specord 250 Plus (Analytik Jena AG, Germany) and plotted vs. concentration. Adsorption capacity was determined using initial and final dye concentrations.

2.2. Adsorbent preparation and characterization

Eggshells were collected from households and restaurants. To eliminate impurities and adhering dust, eggshells were rinsed several times with tap water, and then emerged in distilled water at 25°C for 2 h. The washed material was dried in the dry oven at 100°C for 24 h. The dried eggshells were crushed in a food processor Model 276 (Moulinex, France) and sieved using a laboratory mini sieve shaker (Xinxiang Yongqing, China) to recover the fraction containing particle of sizes between 0.250 and 0.711 mm. Finally, the sieved material was activated with 2N sodium hydroxide NaOH (analytical grade, Merck, China) for 2 h in a heated flask with a reflux condenser. Then the sample was washed until reached neutral pH and dried again in the oven at 100°C for 24 h. The resulted adsorbent is conserved in container for further use and abbreviated as SHTES.

This type of waste has all the favorable characteristics for a promising adsorbent of organic materials after physico-chemical treatment as a final result for this part. The mineral composition of eggshells has a high yield of calcium carbonate (95%) in calcite form, 3.5% organic matter or organic matrix (proteins, polysaccharides and proteoglycans), the eggshells contain also water at 1.5% [29].

The analysis of the X-ray diffractograms (Fig. 1a) using an X'Pert 1 X-Ray diffractometer (Philips, Netherlands) of SHTES shows a sharp and defined peaks which confirms the crystalline structure. The diffractogram of the eggshells shows a main peak at 2θ = 30 with several other small peaks at 2θ = 22.78°, 35.88°, 40.28°, 48°, 49°, 50.85°, 57.48°, 60.74° and 62° which confirms the presence of calcite crystals [30].

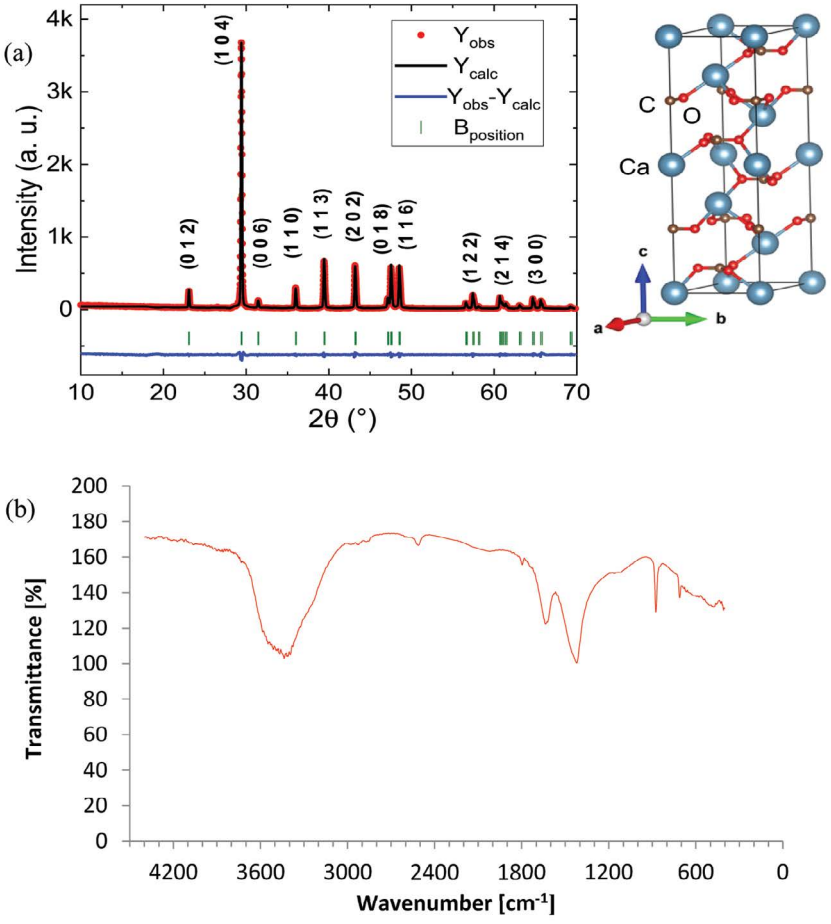

Fig. 1. (a) X-ray diffraction diffractograms of SHTES and (b) FTIR spectrum of SHTES.

Analysis of FTIR Spectrum of SHTES adsorbent was measured using a FTIR spectrometer SP-FTIR-1 (Sco-Tech, Germany) to obtain information on functional groups existing at the adsorbent surface. The spectrum was recorded over wavelengths from 400 to 4,000 cm^{-1} in a sample prepared as KBr pellets under high pressure. Samples were out-gassed at 473 K under vacuum prior to use. SHTES were also characterized by X-ray diffraction using an X'Pert 1 X-Ray diffractometer (Philips, Netherlands).

The analysis of the Fourier-transform infrared spectroscopy (FTIR) spectrum of SHTES (Fig. 1b) shows the stretching and bending vibrations of the functional groups in SHTES relates to the adsorption of the AO7 molecules: The band between 3,600 to 3,700 cm^{-1} is attributed to the binding of OH (water) due to the inter and intra molecular hydrogen bond of NaOH and the polymeric compounds of eggshells, this indication is well confirmed by another band observed between 1,600–1,800 cm^{-1}. The bands between 1,450 and 1,650 cm^{-1} are attributed to the vibrations of C=C bond stretching. The 2,454 cm^{-1} vibration band and the 661 cm^{-1} deformation characterized, respectively, the C–O and CO_2 bond of the atmosphere. The small band located at 1,752 cm^{-1} corresponds to the stretching of the C=O bond, the peak at 2,820 cm^{-1} is due to asymmetric stretching vibrations of C–H. The bands which evolve remarkably in the regions which are situated respectively around 1,400 and 1,500 cm^{-1}, indicating the presence of carbonate minerals within the eggshells matrix [31].

As to evaluate the specific surface area of SHTES adsorbent, Brunauer–Emmett–Teller (BET) multipoint technique is used to describe the multilayer molecular adsorption. The specific surface area calculated using the BET method is found to be 36.60 m^2/g. As reported in previous papers the specific surface area depend on the activation method such as Co_3O_4/SiO_2 (23.7 m^2/g) used for methylene blue elimination [32] and calcined eggshells (CES) (62.42 m^2/g) for basic yellow 28 dye removal [33].

2.3. Column experiments

Continuous-flow experiments for AO7 removal were carried out in a glass fixed-bed column with an internal diameter of 2 cm and a length of 10 cm. A layer of glass wool was placed at the bottom of the column.

1 liter of distilled water was passed through the fixed-bed column in order to remove impurities from the adsorbent prior the use. The influence of different flow rates (2, 4 and 6 ml/min) and AO7 concentrations (30, 50 and 80 mg/L) was investigated. The method of one-factor at-a time was used in this study. The desired flow rate of AO7 solution through the column was provided by a micro peristaltic pump DC12.0V (Makeblock, France). The samples of 1 mL were taken from the outlet of the column at regular time intervals, the adsorbent was separated from the solutions using a cartridge filter and then the AO7 concentration was analyzed as described in section 2.1. The experiments were conducted at temperature of 301 K (28°C ± 1°C) without any pH adjustment (pH = 6.5). Fixed-bed studies were finished when the column achieved exhaustion.

Good design of fixed-bed systems requires predicting the shape of the breakthrough curve for the given effluent, adsorbent and operation conditions. It is usually expressed as a normalized concentration defined as the ratio of outlet to inlet dye concentration (C/C_0) as a function of time.

3. Numerical modeling

3.1. Geometry and mesh

Owing to the symmetry of the problem, the geometry was simplified to 2D axisymmetric system. Fig. 2 illustrates the scheme of the computational domain with z and r representing the vertical and horizontal spatial coordinates, respectively. The diameter and the height of the column are 2 cm and 10 cm respectively.

3.2. Physico-mathematical model

The adsorption of an adsorbate onto an adsorbent in a continuous column is managed by two modes of transfer, the transfer of the momentum energy governed by the Navier–Stokes equations in porous media [Eq. (2)], where the Navier–Stokes equations in a non-porous fluid phase are corrected by introducing the porosity of the medium ϵ in addition to the permeability K_{br} and an inertial loss coefficient β_F obtained from Ergun's equation [34].

$$\rho \nabla u = 0 \tag{1}$$

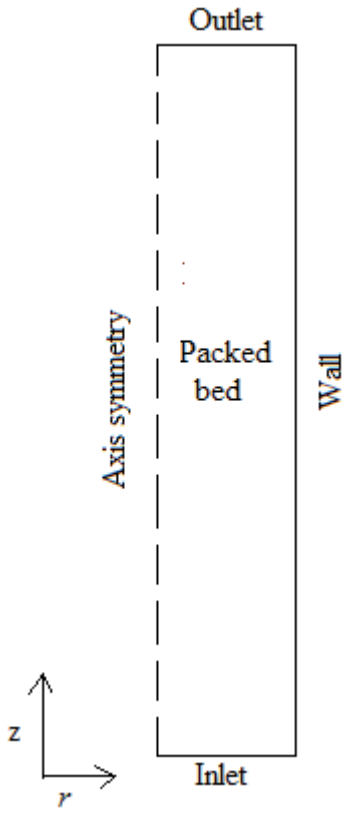

Fig. 2. Computational domain.

$$\frac{\rho}{\varepsilon}\left(\frac{\partial u}{\partial t}+\left(u\nabla\right)\frac{u}{\varepsilon}\right)=\nabla\begin{bmatrix}-pI+\frac{\mu}{\varepsilon}\left\{\left(\nabla u+\left(\nabla u\right)^{T}\right)\right.\\ \left.-\left(\frac{2\mu}{3\varepsilon}\right)\left(\nabla\cdot u\right)I\right\}\\ -\left(\frac{\mu}{k_{\mathrm{br}}}+\beta_{f}\left|u\right|\right)u\end{bmatrix} \tag{2}$$

With

$$k_{\mathrm{br}}=\frac{d_{p}^{2}\varepsilon^{2}}{150\left(1-\varepsilon\right)^{2}} \tag{3}$$

$$\beta_{f}=\frac{3.5-\left(1-\varepsilon\right)}{d_{p}\varepsilon} \tag{4}$$

where ρ is the fluid density, (kg/m^3); v, u are velocity vectors, (m/s); p is the pressure, (Pa); I is identity matrix; μ is the fluid viscosity, Pa·s; ε is the bed porosity and d_p is the particle diameter.

The transfer of solute in the column is governed by Eq. (5) [35,36]. The first term from the left part of the equation represents the non-stationary term, the second term regroups the dispersive and the diffusive term and the last term represents the convective term. Secondly, the dye adsorption on SHTES is represented in the right part of Eq. (3) which is governed by Langmuir law.

$$\left(\varepsilon+\rho_{b}k_{p}\right)\frac{\partial C}{\partial t}+\left(D_{L}+D_{m}\right)\Delta C+u\nabla C=-\left(C-C_{p}\rho_{p}\right)\frac{\partial\varepsilon}{\partial t} \tag{5}$$

with

$$\rho_{p}=\frac{\rho_{b}}{\left(1-\varepsilon\right)} \tag{6}$$

$$k_{p}=\frac{k_{1}q_{p,\max}}{\left(1+k_{1}C\right)^{2}} \tag{7}$$

$$C_{p}=\frac{k_{1}q_{p,\max}C}{1+k_{1}C} \tag{8}$$

where ρ_b is the bulk density, ρ_p is the particle density k_1 is the Langmuir constant, $q_{p,\max}$ is the maximum adsorption, D_L and D_m are the dispersive and the diffusive coefficient, respectively.

3.3. Initial and boundary conditions

Initial and boundary conditions of the model are set as follows:

3.3.1. Equation of movement

At $t = 0$, $u = 0$ and $v = 0$
At $z = 0$, $v = v_e$
With:
$v_e = \dfrac{Q}{A\times\varepsilon}$
At $z = L$, $P = P_{\mathrm{atm}}$

3.3.2. Equation of species

At $t = 0$, $C = 0$
At $z = 0$, $C = C_0$
At $z = L$, $\nabla C = 0$

3.4. Resolution

After the definition of the geometry and the physical model, a finite elements method was used to discretize a set of partial differential Eqs. (1), (2) and (5) into an algebraic equation, with the implementation of a suitable initial and boundary conditions, where the system is automatically solved by an iterative method. The normalized concentration at the outlet of the column is deduced by the average of concentrations at the outlet C divided by the initial concentration C_0. A uniform quadratic mesh is chosen and the introduction of the simulation parameters is established and the time step of the simulation is 10 s. The convergence is established when the error of all the independent variables is less than 10^{-7}. Table 1 presents the simulation parameters.

The equilibrium parameters of Langmuir model for single components and kinetic data used in simulation were estimated from adsorption data of [37,38]. Table 1 illustrates the kinetic data, pore diffusion coefficient and equilibrium parameters for AO7 dye. Laminar flow is assumed, since the Reynold's [Eq. (9)] number is much less than 10 [39].

$$\mathrm{Re}=\frac{d_{p}v_{e}\rho}{\mu} \tag{9}$$

The axial dispersion coefficient D_L of the liquid flowing through a fixed-bed was obtained from the correlation of Chung and Wen [40].

Table 1
Simulation parameters

Parameter	Symbol	Value
Diffusion coefficient, m^2/s	D_m	7.225×10^{-11}
Dispersion coefficient, m^2/s	D_L	Eq. (10)
Bulk density, kg/m^3	ρ_b	223
Liquid density, kg/m^3	ρ	1,000
Particle diameter, m	d_p	0.007
Liquid viscosity, Pa·s	μ	0.001
Bed porosity	ε	0.2
Langmuir constant, L/mg	k_1	0.025
Maximal adsorption, mg/g	$q_{p,\max}$	85

$$D_L = \frac{R_e}{\left(0.2 + 0.011 \times R_e^{0.48}\right)}\left(\frac{\mu}{\rho}\right) \quad (10)$$

4. Results and discussion

A mesh convergence study was established before the start of the simulations. The optimal number of grid nodes is chosen on the basis of mesh independence of the solutions. Table 2 represents the results of the study for two different times (50 and 100 min). Eq. (11) is used to calculate the error in term of concentrations. According to the study, a grid of 100×100 is chosen for all the simulations.

$$E_{\text{mesh}} = \frac{C - C_{125\times125}}{C_{125\times125}} \times 100 \quad (11)$$

Eq. (12) was used to calculate the relative error between experimental and modeling results:

$$E_{\text{tb}} = \left|\frac{t_{b,\text{EXP}} - t_{b,\text{NUM}}}{t_{b,\text{EXP}}}\right| \times 100 \quad (12)$$

4.1. Effect of initial dye concentration

The effect of initial AO7 concentration (30, 50 and 80 mg/L) on the adsorption of AO7 by modified SHTES at fixed-bed column was studied. Constant values of 10 cm and 4 ml/min were used for bed height and flow rate, respectively. Fig. 3 presents the breakthrough curves for the three initial concentrations, the evolution of concentration at the outlet of the column C/C_0 in function of time, obtained using the numerical and the experimental results for the SHTES packed column. It was found that, the trend of the fitted curve agrees well with the experimental breakthrough data. Table 3 presents the breakthrough time t_b, considered approximately at the time ($C/C_0 \approx 0.01$), exhaustion time t_e ($C/C_0 \approx 0.99$), relative error to the breakthrough time [Eq. (12)] and the correlation coefficient between experimental and numerical values. We can observe that the breakthrough time and exhaustion time slightly decreased with increased initial AO7 concentration from 30 to 80 mg/L for the experimental and numerical results, the experimental breakthrough and exhausting times for different dyes concentrations (30, 50 and 80 mg/L) were found as 860, 800, and 760 s for t_b and 6,000, 5,600 and 4,300 s for t_e, respectively. This is due to the increase of the effluent concentration which decreases the adsorption capacity. With the enhancement of the initial ion concentration, the breakthrough curves become much steeper and the breakthrough volume decreased due to the lower driving force in favor of mass-transfer system from the solution to the adsorbent surface and also due to the saturation of the pore distributed on the surface [41].

At lower inlet AO7 concentrations, breakthrough curves were dispersed and became slower. As influent concentration increased, sharper breakthrough curves were obtained. This can be explained by the fact that a lower concentration gradient caused a slower transport due to a decrease in mass transfer coefficient. The larger the inlet concentration, the steeper is the slope of breakthrough curve and the smaller is the breakthrough time and adsorption zone length; this is due to the saturation of SHTES adsorbent at higher initial concentrations [42,43].

The correlation factor (R^2) between the experimental data and the numerical results presented in Table 3 and the error relative to the breakthrough time t_b demonstrates that the results of the numerical model were in good agreement with the experience.

4.2. Effect of flow rate

One of the most important parameters during the evaluation of adsorbents performance in fixed-bed column is the effect of the flow rate [44]. To evaluate this effect on the column performance, experiments were done at three flow rates (2, 4 and 6 ml/min) with initial AO7 concentration of 30 mg/L and bed height of 10 cm. The experimental and numerical resulted breakthrough curves at different flow rates are shown in Fig. 4. As can be seen from this figure, the numerical model predicts accurately the breakthrough curves except for small acceptable deviation due probably to the experimental errors, especially in the case of flow rate 2 ml/min. Nonetheless, prediction for the exhaustion time was in agreement with the experimental data for the studied flow rate. The correlation coefficient (R^2) between the experimental data and the numerical results presented in Table 3 are 0.956, 0.986, and 0.989 for flow rates 2, 4, and 6 ml/min, respectively.

The breakthrough curves (Fig. 4) occurred faster at higher flow rate of 6 ml/min. This is due to the lower residence time to reach the adsorption equilibrium of the influent in the column, thus reducing the contact time between AO7 and the SHTES; so the AO7 solution without occurrence of equilibrium leaves the column. In addition, at higher flow rates, the movement of adsorption zone along the bed is faster reducing the time for adsorption of the dye. The data presented in Table 2 confirmed the observation and indicate that

Table 2
Grid validation C_0 = 30 mg/L, bed height H = 10 cm and flow rates Q = 4 ml/min

Mesh	10 × 10	15 × 15	25 × 25	40 × 40	100 × 100	125×125
C/C_0 (t = 100 min)	0.400	0.424	0.472	0.508	0.530	0.531
Error (%)	24.740	20.094	11.187	4.397	0.290	0.000
C/C_0 (t = 50 min)	0.038	0.041	0.046	0.051	0.054	0.055
Error (%)	31.130	25.765	15.565	6.556	1.264	0.000

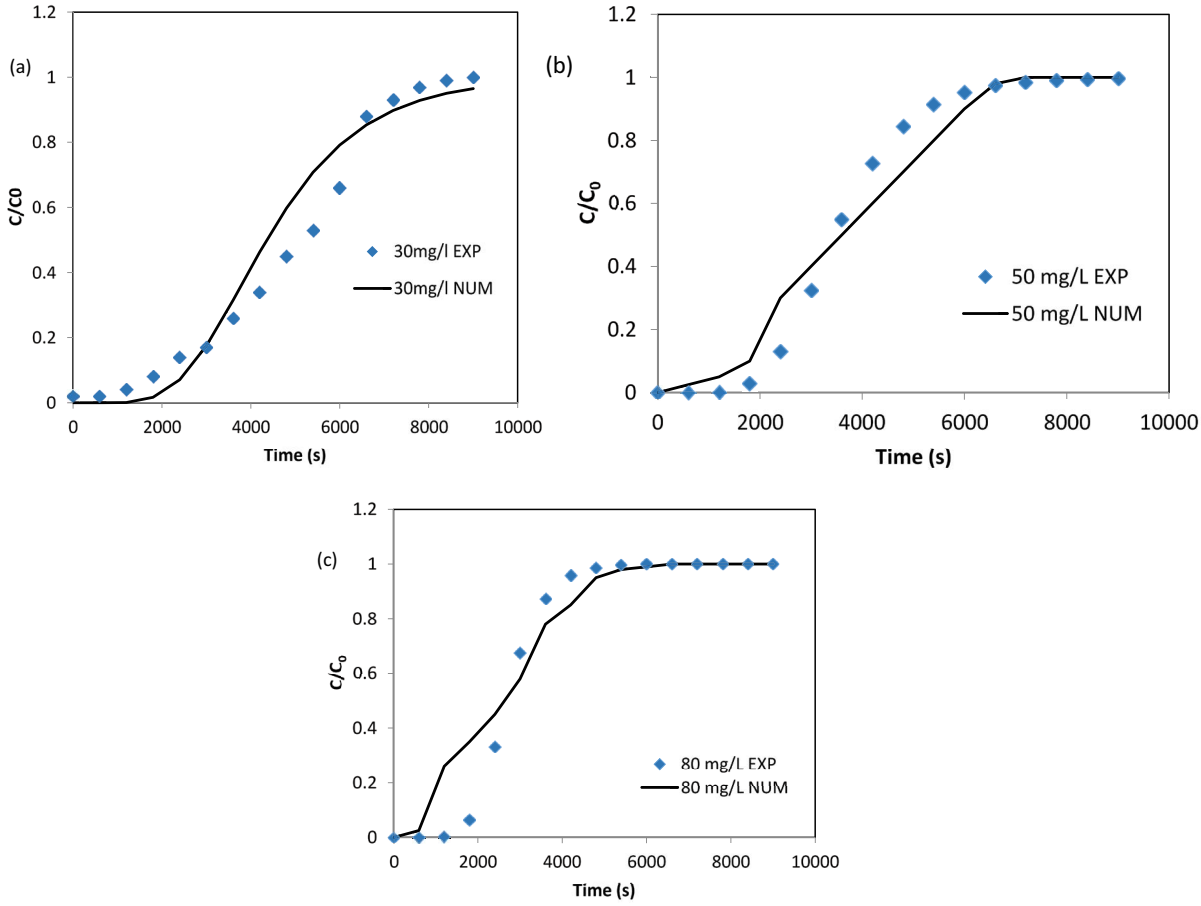

Fig. 3. Comparison of experimental and numerical breakthrough curves for AO7 column adsorption by SHTES. (a) 30 mg/L, (b) 50 mg/L, and (c) 80 mg/L.

Table 3
Breakthrough time, exhaustion time, error and correlation coefficient for different initial concentration and flow rate

Parameter/study	Experimental		Numerical			
Initial concentration (mg/L)	t_b (s)	t_e (s)	t_b (s)	t_e (s)	E_{tb}	R^2
30	860	6,000	900	7,200	4.65	0.982
50	800	5,600	820	5,200	2.50	0.984
80	760	4,300	800	3,950	5.26	0.974
Flow rate (ml/min)						
2	1,800	7,200	2,200	14,400	22.22	0.956
4	830	5,900	900	7,200	8.43	0.986
6	440	4,600	500	4,900	13.63	0.989

breakthrough time t_b decreased significantly for experimental (1,800 to 440 s) and numerical results (2,200 to 500 s) with the increase of the flow rate from 2 to 6 ml/min and in the same way for exhaustion time t_e (7,200 to 4,600 s) and (14,400 to 4,900 s) also for the experimental and numerical results, respectively. In addition, the breakthrough curve for the lower flow rate of 2 ml/min tended to be more gradual which means the column was difficult to be completely exhausted.

The breakthrough of SHTES adsorbent is influenced also by pH which has been investigated in our previous research paper [45] and also by Slimani et al. [46] (pH_{ZPC} = 10.2) in the pH range of 2–11. pH_{ZPC} showed that SHTES presented a negative charge at pH_{ZPC} > 10.2 and a positive charge at pH_{ZPC} < 10.2. Consequently, the higher uptake of AO7 on acidic pH SHTES may be resulted from the electrostatic interactions between species with the different charges, that is, the

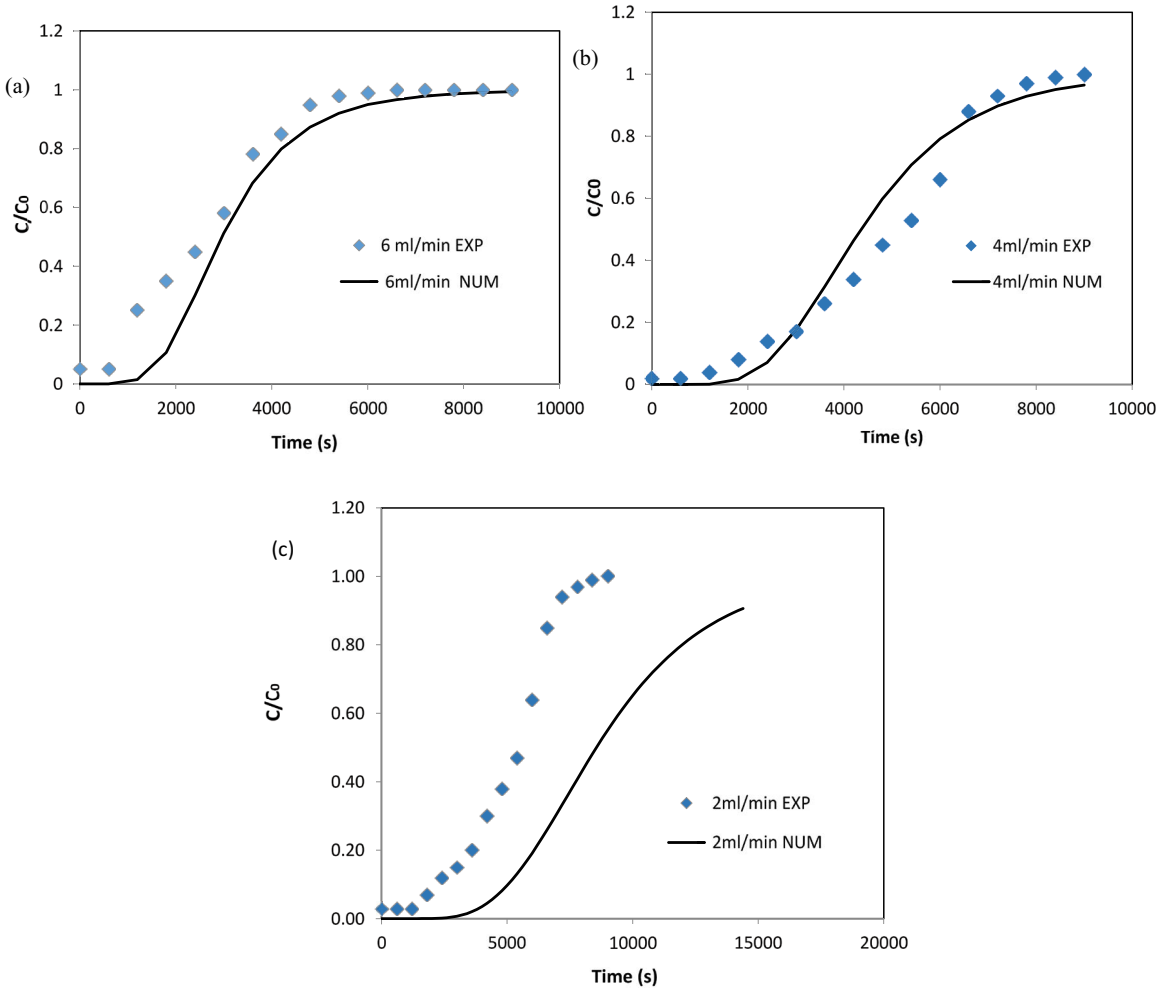

Fig. 4. Comparison of experimental and numerical breakthrough curves of the effect of flow rate on AO7 adsorption onto SHTES column: (a) 6 ml/min, (b) 4 ml/min, and (c) 2 ml/min.

dye molecule and the surface of SHTES [47,48]. The surface of the SHTES contains large number of reactive sites as it confirmed by the relatively high BET surface area (36.60 m^2/g). At lower pH, the surface of the SHTES gets positively charged causing in enhancement in adsorption removal. This can be allocated to the reason that SHTES composition contains functional groups such as hydroxyl groups which protonated in acidic media generating more electrostatic interactions between protonated SHTES and AO7 anionic dye [49,50]. At higher pH, the surface of the SHTES gets negatively charged, which increase the repulsion between AO7 as anionic dye and the surface of our adsorbent.

5. Conclusion

A continuous fixed-bed reactor for wastewater treatment was designed and implemented. The removal of dyes from an aqueous solution on treated eggshell was investigated experimentally and numerically at dynamic conditions for fixed packed columns of 10 cm. A 2D mathematical model with axial symmetry was configured to represent the system of the packed column. The comparison between the experimental and numerical results indicate that the model can be a useful tool to predict the optimum conditions for the adsorption of AO7 dyes liquid on SHTES. Flow rate and initial AO7 concentration effects on the performance of AO7 removal were investigated via the breakthrough curves. The breakthrough and exhaust times were found to decrease with increasing the initial concentration (30, 50 and 80 mg/L) and the flow rate (2, 4 and 6 ml/min) for both experimental and numerical results. The numerical model has demonstrated its capability to predict a breakthrough curves comparable to the experimental ones for AO7 adsorption on SHTES.

Symbols

A	—	Column section, m^2
C	—	Dye concentration, mg/L
C_0	—	Initial dye concentration, mg/L
D_m	—	Diffusion coefficient, m^2/s
D_L	—	Dispersion coefficient, m^2/s
d_p	—	Particle diameter, m
E_{mesh}	—	Mesh error
E_{tb}	—	Breakthrough time error

H	—	Bed height, m
k_L	—	Langmuir constant, L/mg
K_{br}	—	Permeability, m^2
P	—	Pressure, Pa
$q_{q,max}$	—	Maximal adsorption, mg/g
Q	—	Flow rate, ml/min
Re	—	Reynold's number
r	—	Radial spatial coordinate, m
t_b	—	Breakthrough time, s
t_e	—	Exhaustion time, s
u,v	—	Velocity vector, m/s
z	—	Vertical spatial coordinate, m

Greek symbols

β_F	—	Inertial loss coefficient, kg/m^4
ρ_b	—	Bed density, kg/m^3
ρ	—	Liquid density, kg/m^3
ρ_p	—	Particle density, kg/m^3
μ	—	Dynamic viscosity, Pa·s
ε	—	Bed porosity

Abbreviation

NUM	—	Numerical
EXP	—	Experimental
AO7	—	Acid orange 7
SHTES	—	Sodium hydroxide treated eggshells
FTIR	—	Fourier-transform infrared spectroscopy
pHzpc	—	Zero pH charge

References

[1] A.B. dos Santos, F.J. Cervantes, J.B. van Lier, Review paper on current technologies for decolourisation of textile wastewaters: perspectives for anaerobic biotechnology, Bioresour. Technol., 98 (2007) 2369–2385.

[2] B.J. Brüschweiler, C. Merlot, Azo dyes in clothing textiles can be cleaved into a series of mutagenic aromatic amines which are not regulated yet, Regul. Toxicol. Pharm., 88 (2017) 214–226.

[3] B. Naraghi, F. Zabihi, M.R. Narooie, M. Saeidi, H. Biglari, Removal of Acid orange 7 dye from aqueous solutions by adsorption onto Kenya tea pulps; granulated shape, Electron. Physician, 9 (2007) 4312–4321.

[4] W.E. Thung, S.A. Ong, L.N. Ho, Y.S. Wong, F. Ridwan, H.K. Lehl, Y.L. Oon, Y.S. Oon, Biodegradation of Acid orange 7 in a combined anaerobic-aerobic up-flow membrane-less microbial fuel cell: mechanism of biodegradation and electron transfer, Chem. Eng. J., 336 (2018) 397–405.

[5] F. Han, V.S.R. Kambala, R. Dharmarajan, Y. Liu, R. Naidu, Photocatalytic degradation of azo dye Acid orange 7 using different light sources over Fe^{3+}-doped TiO_2 nanocatalysts, Environ. Technol. Innovation, 12 (2018) 27–42.

[6] D. Méndez-Paz, F. Omil, J.M. Lema, Anaerobic treatment of azo dye Acid orange 7 under batch conditions, Enzyme Microb. Technol., 36 (2005) 264–272.

[7] H.M. Xu, X.F. Sun, S.Y. Wang, C. Song, S.G. Wang, Development of laccase/graphene oxide membrane for enhanced synthetic dyes separation and degradation, Sep. Purif. Technol., 204 (2018) 255–260.

[8] D. Morshedi, Z. Mohammadi, M.M.A. Boojar, F. Aliakbari, Using protein nanofibrils to remove azodyes from aqueous solution by the coagulation process, Colloids Surf., B, 112 (2013) 245–254.

[9] S. Singh, S.L. Lo, V.C. Srivastava, A.D. Hiwarkar, Comparative study of electrochemical oxidation for dye degradation: parametric optimization and mechanism identification, J. Environ. Chem. Eng., 4 (2016) 2911–2921.

[10] M. El Ouardi, S. Qourzal, A. Assabbane, J. Douch, Adsorption studies of cationic and anionic dyes on synthetic ball clay, J. Appl. Surf. Interfaces, 1 (2017) 28–34.

[11] N. Arena, J. Lee, R. Clift, Life cycle assessment of activated carbon production from coconut shells, J. Cleaner Prod., 125 (2016) 68–77.

[12] A. Stavrinou, C.A. Aggelopoulos, C.D. Tsakiroglou, Exploring the adsorption mechanisms of cationic and anionic dyes onto agricultural waste peels of banana, cucumber and potato: adsorption kinetics and equilibrium isotherms as a tool, J. Environ. Chem. Eng., 6 (2018) 6958–6970.

[13] G.B. Oguntimein, Biosorption of dye from textile wastewater effluent onto alkali treated dried sunflower seed hull and design of a batch adsorber, J. Environ. Chem. Eng., 3 (2015) 2647–2661.

[14] R. Slimani, I.E. Ouahabi, S. Benkaddour, H. Hiyane, M. Essoufy, Y. Achour, S.E. Antri, S. Lazar, M.E. Haddad, Removal efficiency of textile dyes from aqueous solutions using calcined waste of eggshells as eco-friendly adsorbent: kinetic and thermodynamic studies, Chem. Biochem. Eng. Q., 35 (2021) 43–56.

[15] P.S. Guru, S. Dash, Sorption on eggshell waste—a review on ultrastructure, biomineralization and other applications, Adv. Colloid Interface Sci., 209 (2014) 49–67.

[16] B. Preetha, T. Viruthagiri, Batch and continuous biosorption of chromium(VI) by *Rhizopus arrhizus*, Sep. Purif. Technol., 57 (2007) 126–133.

[17] A. Gabelman, Adsorption Basics: Part 1, American Institute of Chemical Engineers (AIChE), 2017 (Accessed 22 May 2019). Available at: https://www.aiche.org/sites/default/files/docs/pages/adsorption_basics_part_1.pdf

[18] V. Russo, M. Trifuoggi, M. Di Serio, R. Tesser, Fluid solid adsorption in batch and continuous processing: a review and insights into modeling, Chem. Eng. Technol., 40 (2017) 799–820.

[19] A. Hatzikioseyian, M. Tsezos, F. Mavituna, Application of simplified rapid equilibrium models in simulating experimental breakthrough curves from fixed-bed biosorption reactors, Hydrometallurgy, 59 (2001) 395–406.

[20] C.E. Alvarado-Rodríguez, E. Rodríguez-Martínez, J. Klapp-Escribano, R. Duarte-Pérez, M.T. Olguín, A.F. Aguilera-Alvarado, Z. González-Acevedo, Simulation of breakthrough curves of selenium absorbed in two biomass filters using a dispersion and sorption model: use for a hypothetical case, Rev. Mex. Fis., 59 (2013) 258–265.

[21] N. Jurtz, M. Kraume, G.D. Wehinger, Advances in fixed-bed reactor modeling using particle-resolved computational fluid dynamics (CFD), Rev. Chem. Eng., 35 (2019) 139–190.

[22] P. Gaganis, E.D. Skouras, M.A. Theodoropoulou, C.D. Tsakiroglou, V.N. Burganos, On the evaluation of dispersion coefficients from visualization experiments in artificial porous media, J. Hydrol., 307 (2005) 79–91.

[23] W. Qian, J. Wu, L. Yang, X. Lin, Y. Chen, X. Chen, J. Xiong, J. Bai, H. Ying, Computational simulations of breakthrough curves in cAMP adsorption processes in ion-exchange bed under hydrodynamic flow, Chem. Eng. J., 197 (2012) 424–434.

[24] V. Vaiano, O. Sacco, D. Pisano, D. Sannino, P. Ciambelli, From the design to the development of a continuous fixed-bed photoreactor for photocatalytic degradation of organic pollutants in wastewater, Chem. Eng. Sci., 137 (2015) 152–160.

[25] B.H. Xu, A.B. Yu, Numerical simulation of the gas-solid flow in a fluidized bed by combining discrete particle method with computational fluid dynamics, Chem. Eng. Sci., 52 (1997) 2785–2809.

[26] X. Zheng, Y. Liu, L. Wenhai, Two-dimensional modeling of the transport phenomena in the adsorber during pressure swing adsorption process, Ind. Eng. Chem. Res., 49 (2010) 11814–11824.

[27] P. Marin, C.E. Borba, A.N. Módenes, F.R. Espinoza-Quiñones, S.P.D. de Oliveira, A.D. Kroumov, Determination of the mass transfer limiting step of dye adsorption onto commercial adsorbent by using mathematical models, Environ. Technol., 35 (2014) 2356–2364.

[28] N.M. Mahmoodi, M. Arami, K. Gharanjig, Laboratory studies and CFD modeling of photocatalytic degradation of colored textile wastewater by titania nanoparticles, Desal. Water Treat., 1 (2009) 312–317.

[29] Y. Nys, N. Guyot, Chapter 6 – Egg Formation and Chemistry, Y. Nys, M. Bain, F. Van Immerseel, Eds., Improving the Safety and Quality of Eggs and Egg Products, Volume 1: Egg Chemistry, Production and Consumption, Woodhead Publishing Series in Food Science, Technology and Nutrition, Cambridge, UK, 2011, pp. 83–132.
[30] N.H. Sulimai, A.R. Rozina, Z. Khusaimi, S. Abdullah, M.J. Salifairus, A. Salaman, H. Khan, P.A. Sermon, M. Rusop, Facile synthesis of $CaCO_3$ and investigation on structural and optical properties of high purity crystalline calcite, Mater. Sci. Eng. B, 243 (2019) 78–85.
[31] S.T. Maribel, V.B. Lou Andre, C.Q.C. Andrian, B.C. Buenos, C.E. Jimrey, V.G. Jemalyn, O.A. Renato, I.F.M. Val, Efficiency of calcium carbonate from eggshells as an adsorbent for cadmium removal in aqueous solution, Sustainable Environ. Res., 28 (2018) 326–322.
[32] H.H. Abdel Ghafar, A.M.A. Gomaa, A.F. Osama, A.M. Salah, Enhancement of adsorption efficiency of methylene blue on Co_3O_4/SiO_2 nanocomposite, Desal. Water Treat., 53 (2013) 2980–2989.
[33] R. Slimani, I.E. Ouahabi, F. Abidi, M.E. Haddad, A. Regti, M.R. Laamari, S. Lazar, Calcined eggshells as a new biosorbent to remove basic dye from aqueous solutions: thermodynamics, kinetics, isotherms and error analysis, J. Taiwan Inst. Chem. Eng., 45 (2014) 1578–1587.
[34] S. Ergun, Fluid flow through packed columns, Chem. Eng. Prog., 48 (1952) 89–94.
[35] A.H. Sulaymon, S.A. Yousif, M.M. Al-Faize, Competitive biosorption of lead mercury chromium and arsenic ions onto activated sludge in fixed-bed adsorber, J. Taiwan Inst. Chem. Eng., 45 (2014) 325–337.
[36] H. Esfandian, A. Samadi-Maybodi, M. Parvini, B. Khoshandam, Experimental and CFD modeling of diazinon pesticide removal using fixe d b e d column with Cu-modified zeolite nanoparticle, J. Taiwan Inst. Chem. Eng., 65 (2017) 164–173.
[37] M. Arami, Y.N. Limaee, N. Mahmoudi, Investigation on the adsorption capability of eggshell membrane towards model textile dyes, Chemosphere, 65 (2006) 1999–2008.
[38] M.A. Zulfikar, H. Setiyanto, Adsorption of Congo red from aqueous solution using powdered eggshell, Int. J. ChemTech Res., 5 (2013) 1532–1540.
[39] J.P. Holman, Handbook of Heat Transfer, W.M. Rohsenow, J.P. Hartnett, Y.I. Cho, Eds., 3rd ed., McGraw-Hill Education (India) Pvt. Limited, 2002.
[40] O.J. Catchpole, R. Bernig, M.B. King, Measurement and correlation of packed-bed axial dispersion coefficients in supercritical carbon dioxide, Ind. Eng. Chem. Res, 35 (1996) 824–828.
[41] Y. Sun, L.Q.H. Shi, L. Zhang, G.F. Zhao, F.F. Liu, Comprehensive Biotechnology, Reference Module in Life Sciences, 2001, pp. 665–679.
[42] Z. Wang, J. Liu, Y. Dai, W. Dong, S. Zhang, J. Chen, Dimethyl sulfide photocatalytic degradation in a light-emitting-diode continuous reactor: kinetic and mechanistic study, Ind. Eng. Chem. Res., 50 (2011) 7977–7984.
[43] M.E. Farshchi, H. Aghdasinia, A. Khataee, Modeling of heterogeneous Fenton process for dye degradation in a fluidized-bed reactor: kinetics and mass transfer, J. Cleaner Prod., 182 (2018) 644–653.
[44] J.B. Joshi, V.V. Ranade, Computational fluid dynamics for designing process equipment: expectations, current status, and path forward, Ind. Eng. Chem. Res., 42 (2003) 1115–1128.
[45] S. Akazdam, M. Chafi, L. Sebbahi, R. Benchekroune, B. Gourich, N. Barka, Decolourization of Acid orange 7 dye from aqueous solution by adsorption on NaOH treated eggshells in continuous fixed bed reactor application using response surface methodology: optimization by Box–Behnken design, Mor. J. Chem., 6 (2018) 736–751.
[46] R. Slimani, I.E. Ouahabi, S. Benkaddour, H. Hiyane, M. Essoufy, Y. Achour, S.E. Antri, S. Lazar, M.E. Haddad, Removal efficiency of textile dyes from aqueous solutions using calcined waste of eggshells as eco-friendly adsorbent: kinetic and thermodynamic studies, Chem. Biochem. Eng. Q., 35 (2021) 43–56.
[47] A. Arteaga-Jiménez, A.I. Caudana-Campos, A.L. García-García, E. Hernández-Zapata, M.A. Vidales-Hurtado, Adsorption mechanism of Acid orange 7 on photocatalytic materials based on TiO_2, MRS Adv., 4 (2019) 3399–3405.
[48] E.A. Vlasova, N.K. Shalunova, A.S. Makarova, E.V. Kudrik, S.V. Makarov, Metal-organic frameworks based on terephthalic acid: sorbents of organic dyes, Russ. J. Appl. Chem., 87 (2014) 1065–1069.
[49] K.Y.A. Lin, Y.T. Liu, S.Y. Chen, Adsorption of fluoride to UiO-66-NH_2 in water: stability, kinetic, isotherm and thermodynamic studies, J. Colloid Interface Sci., 461 (2016) 79–87.
[50] K.-D. Zhang, F.-C. Tsai, N. Ma, Y. Xia, H.-L. Liu, X.-Q. Zhan, X.-Y. Yu, X.-Z. Zeng, T. Jiang, D. Shi, C.-J. Chang, Adsorption behavior of high stable Zr-based MOFs for the removal of acid organic dye from water, Materials, 10 (2017) 205, doi: 10.3390/ma10020205.